THE JOURNAL OF PHYSICAL CHEMISTRY Letters

Letter

Cite This: J. Phys. Chem. Lett. 2019, 10, 3906−3913

pubs.acs.org/JPCL

Improved Surface Functionalization and Characterization of Membrane-Targeted Semiconductor Voltage Nanosensors

Joonhyuck Park,[†] Yung Kuo,[†] Jack Li,[†] Yi-Lin Huang,[‡] Evan W. Miller,[‡] and Shimon Weiss*[,†,§,∥,⊥]

[†]Department of Chemistry and Biochemistry, University of California Los Angeles, Los Angeles, California 90095, United States

[‡]Department of Chemistry, Department Molecular & Cell Biology, and Helen Wills Neuroscience Institute, University of California Berkeley, Berkeley, California 94720, United States

[§]California NanoSystems Institute, University of California Los Angeles, Los Angeles, California 90095, United States

[∥]Department of Physiology, University of California Los Angeles, Los Angeles, California 90095, United States

[⊥]Department of Physics, Institute for Nanotechnology and Advanced Materials, Bar-Ilan University, Ramat-Gan 52900, Israel

Supporting Information

ABSTRACT: Type-II ZnSe/CdS voltage-sensing seeded nanorods (vsNRs) were functionalized with α-helical peptides and zwitterionic-decorated lipoic acids (zw-LAs). Specific membrane targeting with high loading efficiency and minimal nonspecific binding was achieved. These vsNRs display quantum yield (QY) modulation as a function of membrane potential (MP) changes, as demonstrated at the ensemble level for (i) vesicles treated with valinomycin and (ii) wild-type HEK cells under alternating buffers with different $[K^+]$. $\Delta F/F$ of ∼ 1% was achieved.

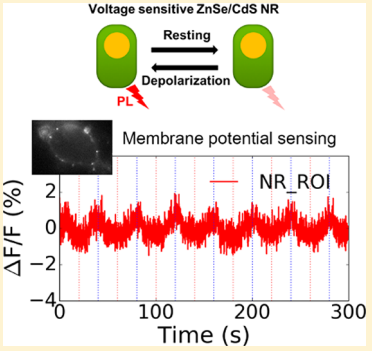

The complex and temporal dynamics in brain systems has been difficult to understand and unravel. In order to untangle the brain activity, tools that allow one to record and interpret the interactions between individual neurons simultaneously need to be developed. Measuring the electrical activity of large neuron populations in brain tissue with high spatial and temporal resolution is crucial to comprehend the dynamics. Numerous technologies for cell membrane potential recording have been developed for decades.

Voltage-sensitive dyes (VSDs) could potentially allow one to visualize the neuronal activity simultaneously over a large number of neurons in a large field-of-view and afford direct imaging of the membrane potential in mammalian brain slices and whole brains of awake mammals.[1−3] However, VSDs could alter membrane capacitance, be phototoxic, and suffer from photobleaching and a short retention time in the membrane.[4] Recently, several genetically encoded voltage indicators (GEVIs) have been developed to detect aggregate neural activity in vivo and the single action potential at the brain tissue level using their fast response kinetics and red emission profile.[5−8] Other types of voltage-sensitive nanoparticles (VSNs) were also reported. Rowland and co-workers elucidated electric field-driven quantum dot (QD) ionization and quasi-type-II QD PL quenching.[9] C60-QD conjugates, modulating their PL by changing of the electron transfer (ET) efficiency between C60 quenchers and QDs, were also developed by Nag et al.[10] We previously demonstrated voltage-sensitive quasi-type-II CdSe/CdS nanorods (NRs) at room temperature (RT) and the single-particle level.[11] We have theoretically evaluated their potential utilization as membrane voltage sensors and examined modes of detections based on intensity changes ($\Delta F/F$), spectral shifts ($\Delta\lambda$), and excited-state lifetime changes ($\Delta\tau$).[12] We showed that when functionalized with transmembrane peptides, voltage-sensing NRs (vsNRs) can be inserted into cellular membranes to report the membrane potential[13] via fluorescence intensity or spectral changes. More recently, we have shown that type-II ZnSe/CdS seeded NRs (CdS nanorods while embedding the ZnSe QDs inside, the same composition as NRs in this paper) exhibit the largest quantum-confined Stark effect (QCSE) among a small library of different composition and shaped nanoparticles. However, we also observed positive correlation between spectral shift ($\Delta\lambda$) and photoluminescence (PL) changes ($\Delta F/F$), in disagreement with usual QCSE predictions, for type-II ZnSe/CdS seeded NRs.[14] We assumed that extrinsic charging/ionization at surface defects of NRs could possibly modulate blinking rates (and hence the quantum yield (QY)) and contribute to the positive $\Delta\lambda$−($\Delta F/F$) correlation. The QCSE could be directly monitored by $\Delta\lambda$ measurements, but $\Delta F/F$ measurements were also affected by extrinsic effects, most likely via QY modulation due

Received: May 2, 2019
Accepted: June 26, 2019
Published: June 26, 2019

to charging and/or ionization at surface and interface defects.[14−16]

Here we further developed and examined vsNRs while focusing on QY modulation (due to charging). These vsNRs could offer unique advantages for sensing the membrane potential: (i) they are very bright and could, in principle, afford single-particle detection; (ii) they display a modulated QY as a function of voltage change across the cell membrane, which presumably originated by charging on the surface's defect; (iii) with an improved surface coating composed of a mixture of α-helical peptides and zwitterionic-decorated lipoic acids (zw-LAs), they could target the cell membrane with high loading efficiency and minimal nonspecific binding. The mixture of peptides and zw-LAs, which contain both positive and negative charges over a wide pH range, provide better colloidal stability to the nanoparticles and decreased nonspecific adsorption as compared to peptide-only coating.[13]

ZnSe/CdS type-II semiconductor NRs were synthesized by the hot-injection method.[17] Briefly, premade ZnSe QDs and octadecanthiol were injected into a solution of cadmium phosphonates at 330 °C. The phosphonic acids in the mixture promote the anisotropic growth of CdS NRs while embedding the ZnSe QDs inside ("seeded NRs").[17] The mixture was kept at ∼320 °C for 15 min to grow NRs and cooled to 50 °C, yielding NRs of 11.8 ± 2.3 nm in length and 6.5 ± 1.5 nm in diameter (# of NRs for the measurement = 50).

To deliver NRs to cell membranes, we improved the previously reported peptide-coating approach.[13] In addition to the modified α-helical transmembrane peptides, we also added zw-LAs[18] to provide colloidal stability. Ligand exchange reaction of the mixture was performed through multiple steps (see the Materials and Methods section for detail). Briefly, as-synthesized NRs (asNRs) were first treated with the ligand stripping agent (triethyloxonium tetrafluoroborate) to remove the original hydrophobic ligands,[19] such as alkylphosphonic acids, alkylphosphine oxides, or alkylamines on the surface of NRs. IR spectroscopy was used to monitor the ligand stripping efficiency. As can be seen in Figure S1, the C−H vibration (2852, 2922 cm^{-1}) and the bending peaks (1466 cm^{-1}) were diminished after the stripping treatment. Next, octanoic acid was added to the NR solution to provide colloidal stability. After removing excess octanoic acid, pyridine was added (acting both as a surface ligand and as a solvent). Pyridine-capped NRs were then mixed with a mixture of 1:3 of zw-LAs:α-helical peptides and redispersed in dimethylsulfoxide(DMSO). The optical properties of these zw-LA-and-peptide (ZAP)-functionalized NRs were preserved after the ligand exchange process, as characterized by UV−vis absorption and fluorescence spectroscopy (emission peak: 605 nm, Figure 1a). The QY of the functionalized ZAP-NRs was only slightly reduced (to 39%) as compared to the original QY of the asNRs (55%). Transmission electron microscopy (TEM) images of the asNRs and the ZAP-NRs showed no substantial change in size after functionalization (Figure 1b,c, long axis = 11.8 ± 2.3 nm and short axis = 6.5 ± 1.5 nm for asNRs, long axis = 12.0 ± 2.4 nm and short axis = 6.7 ± 1.9 nm for ZAP-NRs (# of NRs for the measurement = 50)). The 1:3 ratio of zw-LAs to α-helical peptides was chosen because it was able to provide both colloidal stability and membrane loading efficiency. This ratio is similar to that of the previously reported primary amine-functionalized ligands to zw-LAs ratio used to minimize nonspecific adsorption.[18]

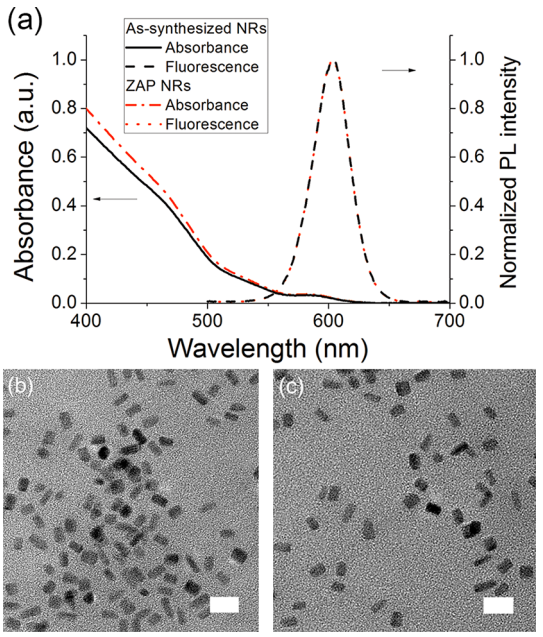

Figure 1. (a) Absorption (black solid) and fluorescence (red dash−dotted) spectra of as-synthesized (black dashed) and ZAP-NRs (red dotted). TEM images of (b) as-synthesized ZnSe/CdS NRs and (c) ZAP-NRs (scale bar: 20 nm).

Interestingly, ZAP-NRs were colloidally stable at 10% and down to 1% DMSO(aq) but started to form aggregates at 0.2% DMSO(aq), as shown by DLS measurements (Figure 2e). The

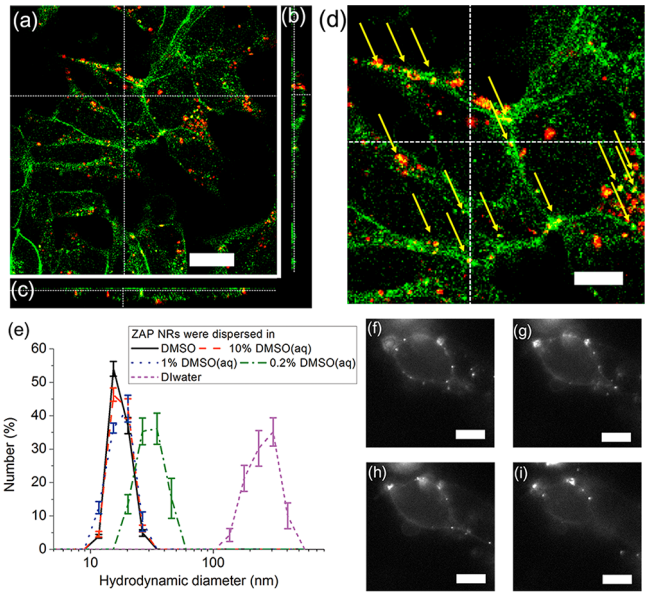

Figure 2. (a) Confocal microscope image of both ZAP-NRs (red) and DiR dye (green) labeled HEK293T cells (scale bar: 20 μm). Cross-sectional images of the (b) *yz* and (c) *xz* plane through the white dotted line in (b). (d) Yellow arrows indicate co-localized ZAP-NRs (yellow signals) with membrane-labeling dyes (green signals) (scale bar: 10 μm). (e) DLS-derived hydrodynamic diameters of ZAP-NRs in DMSO (black solid), 10% DMSO(aq) (red dashed), 1% DMSO(aq) (blue dotted), 0.2% DMSO(aq) (green dash−dotted), and DI water (violet short dashed). (f−i) Wide-field fluorescence images of ZAP-NR-labeled HEK293T cells at different heights from the focal plane (scale bar: 10 μm).

DOI: 10.1021/acs.jpclett.9b01258
J. Phys. Chem. Lett. 2019, 10, 3906−3913

zeta potential of ZAP-NRs was slightly negative (−13.2 ± 2.2 mV at 1% DMSO condition, # of measurement = 10, Figure S2), elucidating to their solubility and colloidal stability. We argue that the amphiphilic nature of the peptides affords the dispersion of ZAP-NRs in DMSO, while the zw-LAs afford their partial solubilization in DI water (Figure S3).

The membrane loading ability and specificity of ZAP-NRs were assessed by confocal microscopy (Figure 2b−d). HEK293T cells were sequentially incubated with 30 nM ZAP-NRs for 1 h (the mean PL intensity from ZAP-NR-labeled HEK cells were saturated after 1 h; flow cytometry data with different incubation time are given in Figure S4) and then with 2 μM DiR membrane-staining dye for 15 min. Next, cells were fixed with 4% paraformaldehyde for 15 min at RT.

At the diffraction-limited resolution of the confocal microscope, ZAP-NRs (red channel) and DiR dye (green channel) seem to be co-localized at the cell membrane (Figure 2a and a zoom-in in Figure 2d), as supported by $y-z$ and $x-z$ cross-sectional images (Figure 2b,c) through the yz or xz planes. Yellow arrows in Figure 2d show the co-localized ZAP-NRs with the membrane, and some of them (red dots) were internalized into HEK cells. Wide-field fluorescence images at different focal planes also support co-localization (Figure 2f−i). At the edge of HEK cells, which would be the cell membrane mainly, there were smaller single ZAP-NRs and also some aggregated ZAP-NRs after their intracellular delivery. We think that these aggregates would not be sensitive under the membrane potential and do not affect the voltage sensitivity of other individual ZAP-NRs.

We were able to observe the ZAP-NRs associated with the membrane after 1 h of incubation, while negatively or positively charged QDs were internalized much faster under similar conditions.[18] We note, however, that these observations report only on the association of ZAP-NRs to membranes; they do not provide evidence for membrane insertion. Nonetheless, functional assays (reported below) do suggest that at least some portion of the ZAP-NRs are inserted into the membrane.

To assess voltage sensitivity (at the ensemble level), ZAP-NRs were loaded into lipid vesicles prepared in a HEPES buffer (20 mM, pH 7.4) with $[K^+]$ = 140 mM and then placed into am isosmotic HEPES buffer (20 mM, pH 7.4) with $[K^+]$ = 2.7 mM. This preparation establishes a potential of −101.4 mV (as determined by the Nernst equation) across the membrane. Valinomycin, a naturally occurring potassium ionophore (extracted from Streptomyces cells) was added at t = 60 s to the vesicles. Once valinomycin was introduced, K^+ ions flowed (from inside to outside of the vesicles) to equalize the $[K^+]$ concentration gradient, thus abolishing the established membrane potential.[20] Vesicle membrane labeling by ZAP-NRs was confirmed by fluorescence microscopy (Figure S5). The ZAP-NRs PL intensity was monitored at 605 nm for 120 s during this process (Figures 3a and S5). Valinomycin was added at t = 60 s. A clear drop in the ZAP-NRs' PL is seen at this time point (red curve), from which we could calculate $\Delta F/F$ = 1.1 ± 0.2% per 100 mV (# of sample = 5; the p value was 0.005 (statistically significant) with the t test under the comparison with the no valinomycin treatment sample). Here, ΔF is defined as the difference between the PL intensity at 605 nm from the sample before and after valinomycin treatment. F is defined as the PL intensity at 605 nm from the sample before valinomycin treatment. The control experiments (no valinomycin added in the same buffer condition (Figure 3a, black circle) or no established membrane potential—by having the same $[K^+]$ = 2.7 mM inside and outside of the vesicle—with valinomycin (Figure 3b, blue circle)) show no change in PL intensity (black and blue curves, respectively, Figure 3a,b). When a full PL spectrum of the ZAP-NRs was recorded, a similar drop of 1% was observed after the addition of valinomycin (Figure S6).

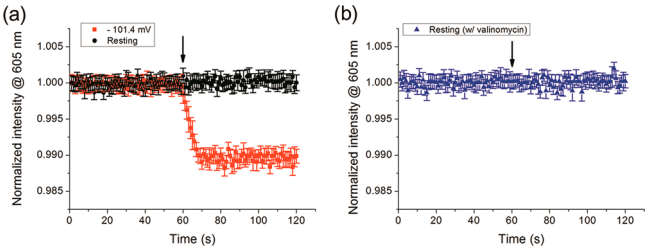

Figure 3. (a) Time-lapse PL intensity measurement of ZAP-NR-labeled vesicles (a) under a membrane potential of −101.4 mV (with $[K^+]$ = 2.7 mM outside and $[K^+]$ = 140 mM inside of the vesicle, red square). This potential was abolished at t = 60 s after valinomycin addition (arrow). If valinomycin is not added, there is no change in the membrane potential (black circle). (b) Control experiment (blue triangle): time-lapse PL intensity measurement of ZAP-NR-labeled vesicles under resting conditions, with $[K^+]$ = 2.7 mM outside and inside of the vesicle; valinomycin was added at t = 60 s (arrow).

Monitoring PL changes as a function of time also allowed us to monitor the time that it takes to establish the resting potential after the introduction of the $[K^+]$ = 140 mM vesicles into the $[K^+]$ = 2.7 mM buffer. The time for balancing the K^+ ion concentration between inside and outside of the vesicle was determined to be 9 s. This time constant is mainly governed by the K^+ ion transfer rate through the ionophore. The drop in PL intensity at around t = 60 s (Figure 3a, after the addition of valinomycin) can be governed by the mixing/diffusion of valinomycin, the binding constant of valinomycin to the membrane, and the K^+ ion transfer rate through the ionophore. A previous work reported 25 s for balancing the difference of $[K^+]$ between inside and outside of a human red blood cell membrane in the presence of valinomycin.[21] We note that PL quenching results for a quasi-type-II QD in a PMMA matrix placed between electrodes and subjected to a synthetic voltage sweep of 20 mV yielded a $\Delta F/F$ of ∼2% from the other's published work.[9] However, the actual field strength in this work could be quite different as compared to our experiment due to differences in local environments.

To evaluate the membrane potential sensitivity of ZAP-NRs under periodic membrane potential modulation, we precultured HEK293T cells in a flow chamber, loaded ZAP-NRs, and recorded PL changes under periodic buffer exchange (of HEPES buffers containing either $[K^+]$ = 2.7 or 140 mM, every 20 s, for 7 cycles). This chemical modulation method establishes cell membrane potential modulation in the presence of valinomycin.[21,22] HEK293T cells were cultured in poly-L-lysine-pretreated flow chambers with six channels. Cells were first treated with 5 μM valinomycin for 5 min. Then 1 μL of ZAP-NRs (3 μM stock, final concentration would be 30 nM) was added to the culture medium of each chamber and incubated for 15 min. To confirm and calibrate the chemical voltage induction in live HEK293T cells, near-infrared (NIR) VSD BeRST[23] (final concentration would be 200 nM) was added to the cells and incubated for 15 min. After each labeling step, excess ZAP-NRs and dyes were removed by a washing

DOI: 10.1021/acs.jpclett.9b01258
J. Phys. Chem. Lett. 2019, 10, 3906−3913

step with Dulbecco Modified Eagle Medium (DMEM) growth media (with 10% fetal bovine serum). Control samples were fixed with 4% paraformaldehyde for 10 min at RT (which disturbs the integrity of the cell membrane and abolishes its membrane potential).

The flow chamber was placed on an inverted fluorescence microscope and connected to an automated controlled flow setup. The high ($[K^+]$ = 140 mM) and low ($[K^+]$ = 2.7 mM) concentrations of potassium buffers were continuously alternated every 20 s while a dual-view (for both BeRST and ZAP-NRs channels) movie was acquired for a duration of 300 s. The excitation intensity was adjusted to 0.2 mW/cm^2 in front of the objective lens. The frame rate was 10 Hz. The slow rise of the signal during each period (~10 s) is likely due to the K^+ ion transfer rate through the ionophore after buffer exchange (denoted by dotted red or blue lines in Figure 4b,c,e;

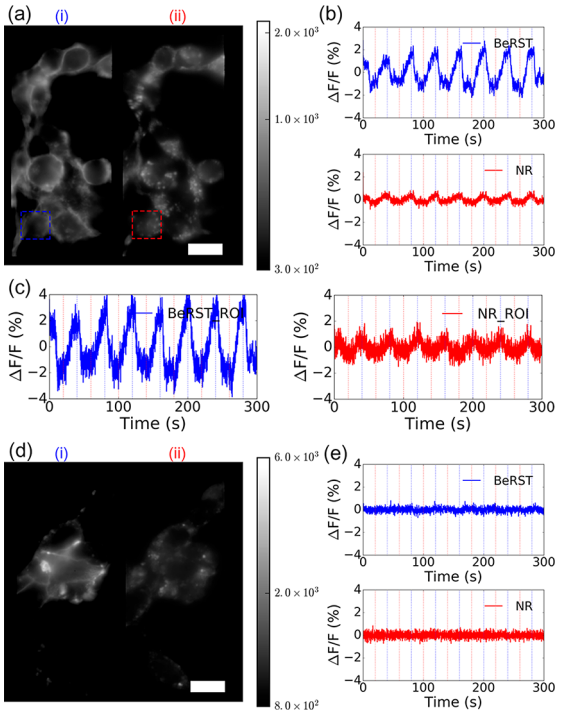

Figure 4. Chemical modulation of the membrane potential of live HEK293T cells. (a) Dual-channel fluorescence microscope images of labeled live HEK293T cells after the addition of valinomycin for (i) the voltage-sensitive BeRST dye channel and for (ii) the ZAP-NRs channel. (d) Dual-channel fluorescence microscope images of labeled fixed HEK293T cells for (i) the BeRST channel and for (ii) the ZAP-NRs channel. (b,e) $\Delta F(t)/F$ for the sum ("ensemble average") of all pixels above a threshold (see method) for BeRST (blue) and ZAP-NRs (red) from (a) and (d), respectively. (c) $\Delta F(t)/F$ from a certain region of interest (one of HEK293T cells) for BeRST (blue) and ZAP-NRs (red) from the dotted area (blue dotted area: BeRST; red dotted area: ZAP-NRs in (a)). Blue or red dotted vertical lines indicate time points for either $[K^+]$ = 2.7 and 140 mM buffer alternation (every 20 s, starting with $[K^+]$ = 2.7 mM at time = 0 s). Scale bar: 20 μm.

overlay graphs of BeRST/ZAP-NRs signals are given in Figure S7). As we mentioned before, a previous report cites a similar 25 s to balance the difference of $[K^+]$ between inside and outside of the human red blood cell membrane.[21]

An "ensemble level" $\Delta F/F$ was calculated from the movie in the following way: First, all pixels above a threshold (Figure S8) per single frame were averaged. This quantity was then averaged over all frames (time points) to yield F. Next, ΔF was defined as the difference between the averaged intensity over all pixels for a single frame (for each time point) and F. The definition of the standard error of the mean (SEM) is the standard deviation of mean values from $\Delta F/F$ values in the same sample group. For the statistics of the chemically modulated experiment in Figure 4, the p value was 0.007 for the ZAP-NR channel and 0.006 for the BeRST channel with the t test (comparison with a fixed HEK293T cell sample for each channel, Figure S9), which is statistically significant, and sample numbers were 20 in all cases. This operation was performed for each spectral channel, yielding $\Delta F/F$ = 3.5 ± 0.3% for BeRST and $\Delta F/F(\pm SEM)$ = 1.0 ± 0.2% for ZAP-NRs per ~200 mV (Figure 4b). The signal-to-noise ratio was defined as the ratio of the peak $\Delta F/F$ value over seven cycles from the sample-to-noise level from the baseline of $\Delta F/F$ from the same sample (Figure 4e). The $\Delta F/F$ values cited above were obtained for signal-to-noise ratios of ~11 and ~5, respectively, and for a membrane potential sweep of −101.4 to +101.4 mV (as determined by the Nernst equation). In terms of absolute brightness, the QY of BeRST in tris buffered saline (TBS)/sodium dodecyl sulfate (SDS) buffer was 2%, and the QY of ZAP-NRs in PBS buffer was 33%. Because the filter setups we were using for either ZAP-NRs or BeRST were different and their brightnesses under the microscope images can be determined by their concentrations, we note that their QYs cannot be extracted directly from the microscope images using our customized setup. To get the signal from a HEK293T cell, $\Delta F/F$ operation from a certain region of interest (ROI, blue dotted area for the BeRST channel and red dotted area for the ZAP-NR channel in Figure 4a) was performed, yielding $\Delta F/F$ = 4.9 ± 0.5% for BeRST and $\Delta F/F$ = 1.8 ± 0.5% for ZAP-NRs (Figure 4c). As the absolute value of $\Delta F/F$ from the ROI of dual-labeled HEK293T cells under voltage sweep increased, the standard deviation of $\Delta F/F$ also increased. Several control experiments were performed in order to validate the above result: (i) The same experiment ($[K^+]$ modulation) was performed for ZAP-NR-labeled, and valinomycin-pretreated, HEK293T cells after fixation (with 4% paraformaldehyde solution at RT for 10 min). Fixation disturbed the integrity of the membrane and abolished its membrane potential. Indeed, no signal modulation was observed for fixed cells (Figure 4d,e). This control eliminates the possibility that the signal originates from direct photophysical property change due to the $[K^+]$ modulation itself, but it is rather due to the membrane potential modulation. (ii) The same experiment ($[K^+]$ modulation) was performed for either ZAP-NRs-only- or BeRST-only-labeled live valinomycin-pretreated HEK293T cells to eliminate the possibility that the ZAP-NRs signal (in doubly labeled cells) originates from the BeRST signal (Figure S9). (iii) The same experiment ($[K^+]$ modulation) was performed for Di-8-ANEPPS-labeled valinomycin-pretreated live HEK293T cells. Di-8-ANEPPS is a well-characterized and -calibrated commercially available VSD, demonstrating similar PL modulation upon $[K^+]$ modulation for cells treated with valinomycin (Figure S10). When the membrane is depolarized, $\Delta F/F$ for Di-8-ANEPPS decreased in a conventional setup, whereas $\Delta F/F$ for BeRST increased.[24−26] However, because we optimized the dichroic cutoff for ZAP-NR spectra and not for Di-8-ANEPPS, the observed $\Delta F/F$ for the latter was 2.1 ± 0.4% (the p value was 0.005 with the t test (comparison with fixed HEK293T cells

DOI: 10.1021/acs.jpclett.9b01258
J. Phys. Chem. Lett. 2019, 10, 3906−3913

sample, Figure S9)), which is statistically significant, and sample numbers were 10). (iv) Solution-based (in vitro) PL measurements of ZAP-NRs as a function of $[K^+]$ (in the range of $[K^+]$ = 0.5−200 mM) and pH (in the range of pH = 5−10) were performed. No significant PL changes were observed (Figure S11a,b). (v) Experiments with no $[K^+]$ modulation were performed on live HEK293T cells treated with valinomycin and doubly labeled with ZAP-NRs and BeRST. No PL modulations were observed (Figure S12a−c). Lastly, (vi) no significant PL changes were observed for nonspecifically adsorbed ZAP-NRs to glass surfaces (Figure S12d−f) upon $[K^+]$ modulation, and no significant autofluorescence changes were observed for unlabeled live HEK293T cells upon $[K^+]$ modulation (Figure S12g−i). The photostability of ZAP-NR-labeled HEK cells was much more stable than BeRST-labeled HEK cells for 10 min under wide-field illumination under a microscope (Figure S13).

The results shown in Figure 4 and the series of control experiments suggest that the $\Delta F/F$ signal reports on the membrane potential modulation at the ensemble level. Although the magnitude of $\Delta F/F$ is very small (∼1%), this result is statistically significant and quite surprising. Our small $\Delta F/F$ is much lower than those of other nanoparticle-based voltage sensors, such as a quasi-type-II QDs in a PMMA matrix placed between electrodes showing $\sim\Delta F/F$ = 2% per 20 mV under a synthetic voltage sweep.[9] Also, QD-C_{60} conjugates have been reported as a membrane potential nanosensor via electron transfer.[10] Their $\Delta F/F$ showed ∼2% in stimulated cortical neurons in mouse cortex and ∼20% in live cultured cells modulated between resting and depolarizing potentials. Even though the $\Delta F/F$ of ZAP-NRs is very small (∼1%), our voltage-sensitive NR showed reversible voltage responsibility under periodic buffer exchange cycles. Moreover, our ZAP-NRs showed their PL turn on in response to depolarization, whereas these nanosensors showed that their PL was turned off.[9,10] Possibly, this unique advantage of our ZAP-NRs provides more sensitive voltage-sensing and a lower false-positive error rate from the photodarkening effect under an electric field.

We previously demonstrated that quasi-type-II CdSe/CdS seeded NRs can report on the membrane potential via the quantum-confined Stark effect (QCSE) at the single-particle level and measured the QCSE for type-II ZnSe/CdS seeded NRs at the single-particle level under in vitro conditions.[14,15] In the later cases, single-particle QCSE measurements exhibited slightly different distributions of positive (43%) and negative (57%) $\Delta F/F$ for randomly oriented type-II ZnSe/CdS seeded NRs. This slight asymmetry could possibly explain the small $\Delta F/F$ measured here on the ensemble level.

We also observed, in disagreement with QCSE predictions, positive correlation between spectral shifts ($\Delta\lambda$) and PL changes ($\Delta F/F$) for type-II ZnSe/CdS seeded NRs.[14] We hypothesized that extrinsic charging/ionization at surface and interface defects[27] could possibly modulate blinking rates (and hence the QY) and contribute to the positive $\Delta\lambda-(\Delta F/F)$ correlation. Such contributions could add up at the ensemble level and therefore be responsible for the ensemble signal observed here. Further studies that correlate spectral, intensity, and lifetime measurements under an applied electric field and at different excitation powers are currently the topic of a follow-up project.

We have demonstrated QY modulation, at the ensemble level, of functionalized and membrane-targeted type-II ZnSe/CdS seeded NRs for vesicles treated with valinomycin and for wild-type HEK cells under alternating buffers with varying K^+ concentrations. $\Delta F/F$ values of ∼1% per 200 mV were achieved. Although the mechanism for these QY modulations is not confirmed as of yet (and is currently under investigation), it is likely not due to the QCSE. Regardless of the mechanism (QCSE or charging/quenching), vsNRs could possibly open up a new nanoneuroscience avenue for high-sensitivity, noise-immune action potential visualization across a large neural network.

MATERIALS AND METHODS

Materials. All chemicals were used as purchased without further purification. Trioctylphosphine oxide (TOPO, 99%), octadecylphosphonic acid (ODPA), and hexylphosphonic acid (HPA) were purchased from PCI Synthesis. Tri-*n*-octylphosphine (TOP, 97%) was obtained from Strem Chemicals. Cadmium oxide (CdO), octadecylamine (ODA), hexadecylamine (HDA), octadecanethiol (ODT), 1.0 M diethylzinc ($Zn(Et)_2$) solution in hexanes, trimethyloxonium tetrafluoroborate (>95%), potassium chloride (KCl), (±)-alpha-lipoic acid (99%), *N*,*N*-dimethylethylenediamine (>98%), 1,3-propane sultone (>98%), tris(2-carboxyethyl)phosphine (TCEP) hydrochloride, anhydrous chloroform, tetramethylammonium hydroxide solution (25% in methanol), dimethyl sulfoxide, and valinomycin (>97%) were purchased from Sigma-Aldrich. Selenium powder (99.999%, 200 mesh) was purchased from Alfa Aesar. Di-8-anepps (D3167), DiR membrane-labeling dye (D12731), phenol-free DMEM, fetal bovine serum, penicillin/streptomycin, and trypsin solution were purchased from Thermo Fisher Scientific. The CG25 peptides were purchased from LifeTein. DOTAP (10 mg/mL in chloroform), DMPC (25 mg/mL in chloroform), and DC-cholesterol (10 mg/mL in chloroform) were purchased from Avanti Polar Lipids.

Preparation of ZnSe/CdS Type-II NRs. The procedure for synthesis of ZnSe QDs was adopted from a previous work.[17] Briefly, a mixture of Se (63 mg), TOP (2 g), and diethyl zinc solution (0.8 mL, 1 M) was injected into degassed HDA (7 g) at 300 °C in an argon atmosphere. The reaction was kept at 265 °C until the desired absorption peak at 360 nm was observed (∼30 min after injection). After the flask was cooled to RT, ZnSe QDs were purified three times by butanol/methanol precipitation and redispersed in toluene. The concentration of ZnSe in toluene was documented by the optical density (OD) at the absorption peak through a 1 cm cuvette.

ZnSe seeded CdS NRs were synthesized using WANDA.[28] CdO (270 mg), ODPA (1305 mg), HPA (360 mg), and TOPO (13.5 g) were first degassed at 100 °C under vacuum for 2 h. The mixture was heated to 230 °C under a nitrogen blanket until CdO powder was dissolved and a colorless solution was obtained. The solution was cooled down to 100 °C, ODA was added (180 mg), and the solution was degassed under vacuum for additional 2 h. To prepare the S precursor solution with ZnSe, 1440 mg of ODT was mixed with 36 units [OD (under 1 cm path length) × mL] of ZnSe solution in toluene and degassed at 100 °C under vacuum to remove the toluene and moisture. After degassing, both the Cd precursor solution and S precursor with ZnSe were transferred under vacuum into a glovebox and dispensed gravimetrically into the 40 mL glass vials used as reaction vessels for the robot. The filled vials were loaded into the eight-reactor array of WANDA, an automated nanocrystal synthesis robot at the Molecular

DOI: 10.1021/acs.jpclett.9b01258
J. Phys. Chem. Lett. 2019, 10, 3906−3913

Foundry. WANDA was used to run up to eight reactions in serial with individually controlled heating/cooling profiles, stirring rates, injections, and aliquot schedules. Below is the description of an exemplary run. Here, 1.133 mL of S/ZnSe solution (heated to 50 °C to prevent solidification) was injected into 15.615 g of Cd solution at 330 °C at a dispense rate of 1.5 mL/s. The temperature after injection was set at 320 °C for CdS NR growth. The heating was stopped 15 min after injection. To thermally quench the reaction, each reaction was then rapidly cooled to 50 °C using a stream of nitrogen, after which 5 mL of acetone was injected.

Functionalization of NRs by zw-LAs and α-Helical Peptides. As-synthesized NRs (100 mg) were mixed with 0.5 mL of stripping agent solution (0.1 M trimethyloxonium tetrafluoroborate in hexane), and the solution was heated to 55 °C for 5 min. It was then spun down (10 000 rcf, 2 min), and the clear supernatant solution containing the NRs was recovered. Next, the solvent was completely removed by vacuum at 50 °C. Then, 0.5 mL of octanoic acid was added to the dried NRs and sonicated for 5 min, 0.1 mL of methanol was added to the NR solution, and the mixture was spun down (10 000 rcf, 2 min). The NRs' precipitate was redispersed in 0.5 mL of pyridine, and 0.2 mL of hexane was added to the NR solution and spun down (10 000 rcf, 2 min). The NRs were then redispersed in 0.5 mL of pyridine. The extinction coefficient of the NRs was determined by ICP-AES measurement to be $\varepsilon = 8 \times 10^6$ L mol cm^{-1}. NRs' absorbance at 400 nm (in pyridine) was used to construct a concentration calibration curve. For the preparation of a 3 μM NR stock solution, 0.1 nmol of NRs in 1 mL of pyridine solution was placed in a glass vial. Then, 3 μmol of the α-helical peptides (CG25, sequence: C_{13}(myristoyl)-CLTCALTCMECTLKCWYKRGCRGCG-carboxylate) in 1.8 mL of DMSO and 10 μL of the zw-LA[18] (from 0.1 M stock solution in DI water), which were reduced by adding 40 μL of tris(2-carboxyethyl)phosphine (TCEP, 0.5 M stock solution in DI water, pH 7.0)), was to the solution. The reduced peptides/zw-LAs mixture was added to the NRs solution in pyridine and vigorously stirred for 10 min. Then, 5 μL of 5% tetramethylammonium hydroxide (TMAOH) solution in methanol was added to the crude NR solution, and the mixture was then spun down (10 000 rcf, 2 min). The precipitate of NRs was redispersed in 33 μL of DMSO and to yield a 3 μM functionalized NRs solution. The NRs' QY was determined by comparison to the known QY of the reference rhodamine 101 (rhodamine 640) dye in methanol (100%). BeRST's QY was determined by comparison to the known QY of the reference cresyl violet in methanol (54%). The PL spectrum of the sample was measured by a PTI QuantaMaster spectrofluorometer (HORIBA).

Cell Culture. HEK293T cells (human embryonic kidney cell line) were maintained in DMEM media (GIBCO) supplemented with 10% (v/v) fetal bovine serum (FBS) and 1% (v/v) penicillin/streptomycin (growth media) for cell adhesion. The culture medium was replaced 24 h prior to imaging and $[K^+]$ modulation experiments with phenol red-free DMEM media supplemented with 10% (v/v) FBS and 1% (v/v) penicillin/streptomycin (imaging media)

Membrane Loading of ZAP-NRs for $[K^+]$ Modulation Experiments. Cultured HEK293T cells (~5000 cells per channel, 6-channel μ-slide chamber, ibidi) were co-incubated with 5 μM valinomycin for 5 min at 37 °C. An excess amount of valinomycin was removed by washing three times with phenol red-free DMEM media. ZAP-NRs (30 nM) were directly added in the DMEM media and incubated for 15 min at RT. For cells dual-labeled with BeRST dye, 200 nM BeRST in DMSO was incubated for 15 min sequentially. Control samples were identically prepared, skipping the valinomycin loading step. For fixation, cells were incubated in 4% paraformaldehyde (in 0.01 M PBS buffer, pH 7.4) for 10 min at RT and washed twice with 0.01 M PBS buffer. For $[K^+]$ modulation experiments, two reservoirs containing $[K^+]$ = 140 and 2.7 mM KCl with 274.6 mM sucrose in HEPES buffer (20 mM, pH 7.4) were connected to a single inlet tube (via a T-connector) of the flow chamber and controlled via computer-controlled valves. The constant flow rate (5 mL/min) was controlled by a peristaltic pump. The outlet of the chamber was connected via another single tube to the waste reservoir. A home-written Labview code controlled the valves via a USB DAQ (USB-6001, National Instruments) and provided a trigger signal to the EMCCD (iXon EM^+ EMCCD, Andor). An "ensemble level" $\Delta F(t)/F$ was calculated in the following way: An "ensemble level" $\Delta F(t)/F$ was calculated from the movie in the following way: First, all pixels above a threshold (Figure S9) per single frame were averaged. This quantity was then averaged over all frames (time points) to yield F. Next, $\Delta F(t)$ was defined as the difference between the averaged intensity over all pixels for a single frame (for each time point) and F.

Optical Imaging. For a dual-view setup in a chemical modulation assay using two different potassium buffers, the microscope setup was based on a Nikon Ti inverted microscope equipped with an LED light source (Aura, Lumencor) and excitation filter (ET470/40×, Chroma Technology Corp). The emissions of the NRs and BeRST dye were collected by ×60 oil immersion, and 1.4 NA objective was used for all imaging experiments. A 530 nm LP emission filter (E530LP, Chroma Technology Corp.) and multiband dichroic mirror (FF545/650-Di01, Semrock) were used to block the LED excitation and pass the emission to the dual-view Optosplit unit (Optosplit II, Cairn Research), which was mounted in front of an Andor iXon EMCCD camera (Andor iXon EM^+, Andor). The optosplit was configured with a 640 nm dichroic (FF640-FDi01, Semrock) and 700 nm LP filters (FELH0700, Thorlab) for the BeRST channel and with a 585/40 bandpass filter (FF01-585/40, Semrock) for the ZAP-NRs channel. The excitation intensity was adjusted to 0.2 mW/cm^2 in front of the objective lens. The frame rate was 10 Hz. Wide-field fluorescence images of ZAP-NR-labeled cells were acquired with a Nikon Ti inverted microscope equipped with an LED light source (Aura, Lumencor) and TxRed filter cube (BP 560/40 for excitation, 595DC, BP 630/60 for emission). Images were recorded with an Ador iXon EMCCD camera (Andor iXon EM^+, Andor).

Co-localization by Confocal Microscopy. HEK293T cells were cultured in glass-bottom dishes (diameter: 35 mm; 3×10^5 cells per dish) and incubated with 30 nM ZAP-NRs for 1 h and with 2 μM DiR dye (D12731, Thermo Fisher Scientific) for 15 min at 37 °C, sequentially. Excess amounts of both the dyes and the NRs were removed by three successive washing steps with phenol red-free DMEM media. The cells were fixed with 4% paraformaldehyde (in 0.01 M PBS buffer, pH 7.4) for 10 min at RT. Fixed cells were washed three times with PBS buffer (0.01 M, pH 7.4) and placed in phenol red-free DMEM media. Confocal images were recorded by an inverted Leica TCS-SP8-SMD confocal microscope at the CNSI's Advanced Light Microscopy/Spectroscopy core facility.

DOI: 10.1021/acs.jpclett.9b01258
J. Phys. Chem. Lett. 2019, 10, 3906−3913

DLS Measurements. ZAP-NR (10 nM as the final concentration) samples were dispersed in 0.2, 1, and 10% DMSO(aq) solutions. For control samples, 100% DMSO and DI water were used as solvents. The Wyatt DynaPro Plate Reader II (Wyatt Technology) was used to acquire DLS data and extract hydrodynamic radii of the samples.

GUVs Preparation and ZAP-NRs Loading for [K$^+$] Modulation Experiments. Giant unilamellar vesicles (GUVs) were prepared according to the following protocol: 6 μL of 1,2-dioleoyl-3-trimethylammonium-propane (chloride salt) (DOTAP, 10 mg/mL in chloroform), 6 μL of 1,2-dimyristoyl-*sn*-glycero-3-phosphocholine (DMPC, 25 mg/mL in chloroform), and 6 μL of (3ß-[*N*-(*N*′,*N*′-dimethylaminoethane)-carbamoyl]-cholesterol hydrochloride, DC-cholesterol, 10 mg/mL in chloroform) were mixed in a glass vial, and chloroform was removed under vacuum at RT. HEPES buffer (1 mL, 20 mM, pH 7.4) with KCl ([K$^+$] = 140 mM) was added to the dried lipids in the glass vial and incubated at 37 °C for 24 h. The vial was vigorously shaken and stored at 37 °C for 24 h to form GUVs. For ZAP-NRs labeling, 1 μL of ZAP-NRs stock solution (3 μM) was treated to the GUVs and incubated for 5 min. To build up the membrane potential, 1 μL of GUV solution was diluted in 1 mL of HEPES buffer (20 mM, pH 7.4) with KCl ([K$^+$] = 2.7 mM with 274.6 mM sucrose). Valinomycin was added after 60 s from the starting time to acquire PL data of ZAP-NR-loaded GUVs. The time-lapse PL intensity of each sample for 120 s at the ZAP-NR peak wavelength (605 nm) was measured by a PTI QuantaMaster spectrofluorometer (HORIBA).

In Vitro PL Measurements of ZAP-NRs as a Function of [K$^+$] and pH. PL measurements of ZAP-NRs as a function of [K$^+$]: 300 nM of ZAP-NRs were placed in 0, 0.5, 1, 2, 5, 10, 20, 50, 100, and 200 mM potassium chloride containing HEPES buffer. To maintain a constant ionic strength, 400, 399, 398, 396, 390, 380, 360, 300, 200, and 0 mM sucrose was dissolved and added to each HEPES buffer, respectively. The PL spectrum of each sample was measured by a PTI QuantaMaster spectrofluorometer (HORIBA).

PL measurements of ZAP-NRs as a function of pH: 300 nM ZAP-NRs were placed in pH 4, 6, 7.4, 8, and 10 buffer (for pH 4: 50 mM acetate buffer; for pH 6 and 7.4: 50 mM MES buffer; for pH 8 and 10: 50 mM PBS buffer). The PL spectrum of each sample was measured by a PTI QuantaMaster spectrofluorometer (HORIBA).

Flow Cytometry Analysis. To investigate the labeling efficiency of ZAP-NRs, HEK293T cells were cultured, and they were co-incubated with the ZAP-NRs. The cells were grown in DMEM growth media for cell adhesion. To optimize the labeling efficiency of ZAP-NRs, 5×10^4 HEK293T cells were cocultured with the 30 nM ZAP-NRs for 15, 30, 45, 60, 90, or 120 min in phenol red-free DMEM media. The cells were detached by adding a 0.25% trypsin and EDTA solution. The cells were then rinsed with PBS buffer (0.1 M, pH 7.4) with 1% FBS (flow cytometry buffer) three times and redispersed in fixing buffer (1% formaldehyde in flow cytometry buffer). The collected cells were further analyzed with flow cytometry.

■ ASSOCIATED CONTENT

Supporting Information

The Supporting Information is available free of charge on the ACS Publications website at DOI: 10.1021/acs.jpclett.9b01258.

Infrared spectrum of type-II ZnSe/CdS NR samples, zeta potential and dynamic light scattering plot of NRs, flow cytometry data of ZAP-NR-labeled HEK cells, wide-field microscope image of ZAP-NR-labeled GUVs, PL spectrum of ZAP-NR-labeled vesicles, $\Delta F(t)/F$ plot and threshold mask image of both BeRST dye and ZAP-NR-labeled HEK cells under seven cycles of chemical modulation, control experiments for chemical modulation in the HEK cell membrane potential, in vitro PL measurements in various [K$^+$] and pH ranges, and photostability plot of both BeRST dye and ZAP-NR-labeled cells (PDF)

■ AUTHOR INFORMATION

ORCID

Joonhyuck Park: 0000-0003-1509-724X
Yung Kuo: 0000-0001-6704-6722
Evan W. Miller: 0000-0002-6556-7679
Shimon Weiss: 0000-0002-0720-5426

Author Contributions

J.P. conducted all experiments, analyzed all of the data, and wrote the manuscript. J.P., Y.K., and J.L. synthesized ZnSe/CdS NRs using WANDA. Y.K. and J.P. developed the cell assay and built the flow setup. S.W., J.P., and Y.K. designed the experiments. Y.-L. H. and E.W.M. provide BeRST dye. S.W., E.W.M., and Y.K. helped in writing and revising the manuscript. All authors have given approval to the final version of the manuscript.

Notes

The authors declare the following competing financial interest(s): S.W., Y.K., and J.L. are inventors on a U.S. Provisional Patent application submitted by the University of California, Los Angeles (Application No. 62504307, filed Oct 5, 2017).

■ ACKNOWLEDGMENTS

We acknowledge Dr. H. Ronald Kaback for assisting with the chemically driven cell membrane modulation assay. We acknowledge Dr. Emory Chan for help with the WANDA instrument. We acknowledge the help of Antonino Ingargiola for processing data from the modulation assay. We also acknowledge the use of instruments at the Electron Imaging Center for NanoMachines supported by the NIH (1S10RR23057 and GM071940 to Z.H.Z.) and the Advanced Light Microscopy/Spectroscopy core, both at the California NanoSystems Institute at the University of California, Los Angeles. Lastly, we acknowledge the participation in the USER Program (#1726 and #3244) of the Molecular Foundry at the Lawrence Berkeley National Laboratory, which was supported by the U.S. Department of Energy Office of Science, Office of Basic Energy Sciences under Contract No. DE-AC02-05CH11231. S.W. acknowledges funding from the United States–Israel Binational Science Foundation (#2010382), the Human Frontier Science Program (#RGP0061/2015), the Defense Advanced Research Projects Agency/Biological Technologies Office Award No. #D14PC00141, the European Research Council (ERC) advanced Grant NVS #669941, and the BER program of the Department of Energy Office of Science, Grant # DE-FC03-02ER63421. This work was also supported by STROBE: A National Science Foundation Science & Technology Center under Grant No. DMR

DOI: 10.1021/acs.jpclett.9b01258
J. Phys. Chem. Lett. 2019, 10, 3906−3913

1548924. E.W.M. acknowledges support from the NIH (R35GM119855).

REFERENCES

(1) Wu, J. Y.; Cohen, L. B.; Falk, C. X. Neuronal Activity during Different Behaviors in Aplysia: A Distributed Organization? *Science* **1994**, *263*, 820.
(2) Grinvald, A.; Hildesheim, R. VSDI: a new era in functional imaging of cortical dynamics. *Nat. Rev. Neurosci.* **2004**, *5*, 874−885.
(3) Peterka, D. S.; Takahashi, H.; Yuste, R. Imaging Voltage in Neurons. *Neuron* **2011**, *69*, 9−21.
(4) Preuss, S.; Stein, W. Comparison of Two Voltage-Sensitive Dyes and Their Suitability for Long-Term Imaging of Neuronal Activity. *PLoS One* **2013**, *8*, No. e75678.
(5) St-Pierre, F.; Marshall, J. D.; Yang, Y.; Gong, Y.; Schnitzer, M. J.; Lin, M. Z. High-fidelity Optical Reporting of Neuronal Electrical Activity with An Ultrafast Fluorescent Voltage Sensor. *Nat. Neurosci.* **2014**, *17*, 884.
(6) Gong, Y.; Huang, C.; Li, J. Z.; Grewe, B. F.; Zhang, Y.; Eismann, S.; Schnitzer, M. J. High-speed Recording of Neural Spikes in Awake Mice and Flies with a Fluorescent Voltage Sensor. *Science* **2015**, *350*, 1361.
(7) Kannan, M.; Vasan, G.; Huang, C.; Haziza, S.; Li, J. Z.; Inan, H.; Schnitzer, M. J.; Pieribone, V. A. Fast, in vivo Voltage Imaging Using a Red Fluorescent Indicator. *Nat. Methods* **2018**, *15* (12), 1108−1116.
(8) Abdelfattah, A. S.; Kawashima, T.; Singh, A.; Novak, O.; Liu, H.; Shuai, Y.; Huang, Y.-C.; Grimm, J. B.; Patel, R.; Friedrich, J.; et al. Bright and Photostable Chemigenetic Indicators for Extended in vivo Voltage Imaging. *bioRxiv* **2018**, 436840.
(9) Rowland, C. E.; Susumu, K.; Stewart, M. H.; Oh, E.; Mäkinen, A. J.; O'Shaughnessy, T. J.; Kushto, G.; Wolak, M. A.; Erickson, J. S.; L. Efros, A.; et al. Electric Field Modulation of Semiconductor Quantum Dot Photoluminescence: Insights Into the Design of Robust Voltage-Sensitive Cellular Imaging Probes. *Nano Lett.* **2015**, *15*, 6848−6854.
(10) Nag, O. K.; Stewart, M. H.; Deschamps, J. R.; Susumu, K.; Oh, E.; Tsytsarev, V.; Tang, Q.; Efros, A. L.; Vaxenburg, R.; Black, B. J.; et al. Quantum Dot−Peptide−Fullerene Bioconjugates for Visualization of in Vitro and in Vivo Cellular Membrane Potential. *ACS Nano* **2017**, *11*, 5598−5613.
(11) Park, K.; Deutsch, Z.; Li, J. J.; Oron, D.; Weiss, S. Single Molecule Quantum-Confined Stark Effect Measurements of Semiconductor Nanoparticles at Room Temperature. *ACS Nano* **2012**, *6*, 10013−10023.
(12) Park, K.; Weiss, S. Design Rules for Membrane-Embedded Voltage-Sensing Nanoparticles. *Biophys. J.* **2017**, *112*, 703−713.
(13) Park, K.; Kuo, Y.; Shvadchak, V.; Ingargiola, A.; Dai, X.; Hsiung, L.; Kim, W.; Zhou, H.; Zou, P.; Levine, A. J.; et al. Membrane insertion of—and membrane potential sensing by—semiconductor voltage nanosensors: Feasibility demonstration. *Sci. Adv.* **2018**, *4*, No. e1601453.
(14) Kuo, Y.; Li, J.; Michalet, X.; Chizhik, A.; Meir, N.; Bar-Elli, O.; Chan, E.; Oron, D.; Enderlein, J.; Weiss, S. Characterizing the Quantum-Confined Stark Effect in Semiconductor Quantum Dots and Nanorods for Single-Molecule Electrophysiology. *ACS Photonics* **2018**, *5*, 4788−4800.
(15) Bar-Elli, O.; Steinitz, D.; Yang, G.; Tenne, R.; Ludwig, A.; Kuo, Y.; Triller, A.; Weiss, S.; Oron, D. Rapid Voltage Sensing with Single Nanorods via the Quantum Confined Stark Effect. *ACS Photonics* **2018**, *5*, 2860−2867.
(16) Efros, A. L.; Delehanty, J. B.; Huston, A. L.; Medintz, I. L.; Barbic, M.; Harris, T. D. Evaluating the Potential of Using Quantum Dots for Monitoring Electrical Signals in Neurons. *Nat. Nanotechnol.* **2018**, *13*, 278−288.
(17) Dorfs, D.; Salant, A.; Popov, I.; Banin, U. ZnSe Quantum Dots Within CdS Nanorods: A Seeded-Growth Type-II System. *Small* **2008**, *4*, 1319−1323.
(18) Park, J.; Nam, J.; Won, N.; Jin, H.; Jung, S.; Jung, S.; Cho, S.-H.; Kim, S. Compact and Stable Quantum Dots with Positive, Negative, or Zwitterionic Surface: Specific Cell Interactions and Non-Specific Adsorptions by the Surface Charges. *Adv. Funct. Mater.* **2011**, *21*, 1558−1566.
(19) Rosen, E. L.; Buonsanti, R.; Llordes, A.; Sawvel, A. M.; Milliron, D. J.; Helms, B. A. Exceptionally Mild Reactive Stripping of Native Ligands from Nanocrystal Surfaces by Using Meerwein's Salt. *Angew. Chem., Int. Ed.* **2012**, *51*, 684−689.
(20) Montana, V.; Farkas, D. L.; Loew, L. M. Dual-wavelength Ratiometric Fluorescence Measurements of Membrane Potential. *Biochemistry* **1989**, *28*, 4536−4539.
(21) Bifano, E. M.; Novak, T. S.; Freedman, J. C. Relationship between the Shape and the Membrane Potential of Human Red Blood Cells. *J. Membr. Biol.* **1984**, *82*, 1−13.
(22) Kao, L.; Azimov, R.; Shao, X. M.; Frausto, R. F.; Abuladze, N.; Newman, D.; Aldave, A. J.; Kurtz, I. Multifunctional Ion Transport Properties of Human SLC4A11: Comparison of the SLC4A11-B and SLC4A11-C Variants. *Am. J. Physiol. Cell Physiol.* **2016**, *311*, C820−C830.
(23) Huang, Y.-L.; Walker, A. S.; Miller, E. W. A Photostable Silicon Rhodamine Platform for Optical Voltage Sensing. *J. Am. Chem. Soc.* **2015**, *137*, 10767−10776.
(24) DiFranco, M.; Capote, J.; Vergara, J. L. Optical Imaging and Functional Characterization of the Transverse Tubular System of Mammalian Muscle Fibers using the Potentiometric Indicator di-8-ANEPPS. *J. Membr. Biol.* **2005**, *208*, 141−153.
(25) Kao, W. Y.; Davis, C. E.; Kim, Y. I.; Beach, J. M. Fluorescence Emission Spectral Shift Measurements of Membrane Potential in Single Cells. *Biophys. J.* **2001**, *81*, 1163−1170.
(26) Manno, C.; Figueroa, L.; Fitts, R.; Ríos, E. Confocal Imaging of Transmembrane Voltage by SEER of di-8-ANEPPS. *J. Gen. Physiol.* **2013**, *141*, 371−387.
(27) Park, S.-J.; Link, S.; Miller, W. L.; Gesquiere, A.; Barbara, P. F. Effect of Electric Field on the Photoluminescence Intensity of Single CdSe Nanocrystals. *Chem. Phys.* **2007**, *341*, 169−174.
(28) Chan, E. M.; Xu, C.; Mao, A. W.; Han, G.; Owen, J. S.; Cohen, B. E.; Milliron, D. J. Reproducible, High-Throughput Synthesis of Colloidal Nanocrystals for Optimization in Multidimensional Parameter Space. *Nano Lett.* **2010**, *10*, 1874−1885.

DOI: 10.1021/acs.jpclett.9b01258
J. Phys. Chem. Lett. 2019, 10, 3906−3913